The Effects of Inorganic Arsenic On Apoptosis and Autophagy in Human Hepatic Sellate Cells

Fei Huang
Xinjiang Medical University
Yu Hui
Xinjiang Second Medical College
Ang Li
Xinjiang Medical University
Rishalaiti Tayier
Xinjiang Medical University
Dilinaer Yaermaimaiti
Xinjiang Medical University
Guanxin Ding
Xinjiang Medical University
Shunhua Wu (xjmuketizu@163.com)
Xinjiang Medical University

Research Article

Keywords: inorganic arsenic, liver fibrosis, autophagy, 3-methyladenine, apoptosis pathways

Posted Date: January 11th, 2022

DOI: https://doi.org/10.21203/rs.3.rs-1145060/v1

Abstract

Endemic arsenism is a major disease concern in China, with arsenic poisoning and induced potential lesions key issues on a global level. The liver is the main target organ where arsenic is metabolized; chronic exposure to arsenic-induced liver fibrosis is also closely related to autophagy, however, the exact mechanisms are remain unclear. In this study, we explored the effects of $NaAsO_2$ on apoptosis and autophagy in human hepatic stellate cells(HSC). We established a fibrosis model in the HSC line, LX-2 which was exposed to $NaAsO_2$ for 24h, 48h, and 72h. Cells were then transfected using an autophagy double-labeled RFP-GFP-LC3 adenoviral plasmid. Laser confocal microscopy indicated significant infection efficiencies and autophagy in LX-2. Flow cytometry was also used to investigate the effects of different $NaAsO_2$ doses on apoptosis. $NaAsO_2$ treatment upregulated the expression of autophagic markers, including microtubule-associated protein light chain A/B(LC3), ubiquitin binding protein(SQSTM-1/P62), autophagy related genes(ATGs), recombinant human autophagy effector protein (Beclin-1), and B cell lymphoma-2(BCL-2), but downregulated mammalian target of rapamycin(mTOR). Also, α-smooth muscle actin(α-SMA) expression was significantly upregulated in all $NaAsO_2$ groups. Furthermore, mTOR silencing via 3-methyladenine(3-MA) altered $NaAsO_2$ induced autophagy, LC3, Beclin-1, and SQSTM-1/P62 expression were all upregulated in both $NaAsO_2$ and 3-MA-iAs groups. Altogether, $NaAsO_2$ induced HSC autophagy via apoptotic pathways. 3-MA inhibited LX-2 activity and reduced $NaAsO_2$-induced autophagy which may inhibit fibrosis progression caused by this toxin.

1. Introduction

Endemic arsenic disease is a serious environmental and geochemical issue endangering human health[1].According to 2016 statistics, nearly 150 million people in more than 70 global regions were variably threatened by high arsenic groundwater levels[2]. Inorganic arsenic (iAs) is a ubiquitously distributed environmental and industrial toxicant, designated a class I carcinogen by the International Cancer Research Institute and the United States Environmental Protection Agency[3]. Arsenic has two oxidation states in the environment. iAs as a potential environmental carcinogen is not only associated with multiple cancers (skin[4], lung[5], liver[6], kidney[7], and bladder[8]), but is also detrimental to multiple organ systems, including the liver and kidneys, cardiovascular, respiratory, and reproductive systems[9]. The liver is the most important target organ of arsenic metabolism[10]. Epidemiological studies have linked chronic iAs exposure to an increased risk of liver disease, fibrosis, cirrhosis, and liver carcinogenesis[11–13]. Arsenic carcinogenic mechanisms mainly relate to oxidative stress, DNA and chromosome damage, apoptosis, necrosis, and methylation. Importantly, in recent years, studies have also reported that autophagy plays a vital role in arsenic-related carcinogenic mechanisms[14].

Autophagy is a conserved, tightly regulated process with key roles in protein and organelle quality control via intracellular molecule capture, degradation, and recycling[15]. The process is characterized by macroautophagy, microautophagy, and chaperone-mediated autophagy mechanisms[16]. Significantly,

arsenic exposures affects cellular autophagy in a dose-dependent manner[17]. Multiple autophagy-related genes (ATGs) and signaling pathways co-regulate autophagy processes and biological functions[18]. Currently, 42 ATGs have been identified, with autophagy processes closely related to key signaling molecules, including, Beclin-1, VMP1, Atg5–Atg12, Atg4, and LC3, and also regulated by signal transduction pathways, including molecular target of rapamycin (mTOR), and phosphatidylinositol 3 kinase/protein serine threonine kinase (PI3K-Akt)[19,20]. In this study, a comprehensive and reliable autophagy quantitative analytical method was required to investigate these complex mechanisms, therefore, we developed a double fluorescence RFP-GFP-LC3 system. The biggest advantage of the system is that no drug interventions are required, only a hunger-induced (serum-free medium) starvation mechanism is necessary to visually determine changes in autophagic activity and autophagic flow (autophagic flux). Thus using this strategy, autophagy was observed by fluorescence, indicating the successful construction of an RFP-GFP-LC3 lentivirus system in this study.

The effects of arsenic poisoning on liver fibrosis have been characterized but underlying mechanisms are unclear[21]. Autophagy as a fundamental degradation pathway in eukaryotic cells also induces liver fibrosis; hepatic stellate cell (HSC) activation contributes to liver fibrosis where autophagy processes provide energy for HSC activation by degrading lipid droplets, thereby promoting fibrosis[22]. In rat lungs, a high arsenic exposure (up to 10 μg/L) to drinking water triggered inflammation, oxidative damage, and inhibited autophagy[23]. Moderate autophagy helped cell survival and protected cells from dysfunction[24], but excessive autophagy resulted in the gradual consumption of cell capacity, resulting in autophagic death[25].

3-Methyladenine (3-MA) is a phosphatidylinositol 3-kinases (PI3K) inhibitor. PI3K plays key roles in several biological processes, including controlling mTOR activation which is a key autophagy regulator. Also, 3-MA inhibits autophagy by blocking autophagosome formation by inhibiting class III PI3Ks[26]. Similarly, 3-MA plays a dual role in autophagy; prolonged 3-MA treatment promotes autophagy under nutrient-rich conditions, whereas 3-MA inhibits starvation-induced autophagy[27]. The inhibitor also prevents liver fibrosis by downregulating autophagy levels and inhibiting liver fibrosis progression caused by carbon tetrachloride (CCL4)[28]. However, it is currently unclear if 3-MA inhibits arsenic-mediated fibrosis, therefore we investigated this phenomenon in this study.

In this study, we assessed HSC responses to different iAs^{3+} doses to characterize the full range of chronic arsenic exposure levels. Then, we investigated changes in autophagy protein levels during iAs^{3+}-induced fibrosis. Finally, we silenced mTOR using 3-MA to alter iAs^{3+}-induced autophagy. Our data may be used as a platform to explore changes in autophagy related-proteins during iAs-induced fibrosis in human HSCs, and importantly, lays a foundation for further liver fibrosis investigations.

2. Materials And Methods

2.1. Reagents and antibodies

The following reagents were used in this study. Sodium arsenite (iAs^{3+}, analytical grade) (No.3 Chemical Reagent Factory, Beijing, China). RFP-GFP-LC3 lentivirus (Jikai Gene Biology Co. Shanghai China). The double fluorescence RFP-GFP-LC3 autophagy system was used in this research. The primary advantage of the system is the absence of any drug intervention to induce autophagy, instead, hunger (serum-free medium) induces changes in autophagy activity and autophagy flow (autophagic flux) and visualized under fluorescence microscopy. Once the system was authenticated, control and arsenic exposure groups were tested under normal and starvation conditions. Concomitant with changes in autophagy, we observed transcription and translation changes in autophagy-related genes, demonstrating that autophagy after arsenic exposure was independent of hunger, but that arsenic affected autophagy.

The real-time monitoring of RFP-GFP-LC3 adenovirus; RFP labeled and tracked LC3, whereas weakened GFP indicated lysosome and autophagosome fusion to form an autophagic lysosome. As GFP fluorescence was acid sensitive, GFP quenching occurred when the autophagosome and lysosome fused, therefore only red fluorescence was detected. This fluorescent protein expression system clearly indicated levels of autophagy flow and was an indispensable tool for our autophagy studies. Fetal bovine serum (FBS) and Dulbecco's modified eagle medium (DMEM) (American Hyclone Co.), Bicinchoninic acid assay (BCA) protein quantification kit (Thermo Scientific, USA). Electrotransfer and electrophoresis solution (Solarbio Co. Beijing, China). Annexin V-PE apoptosis detection kit I (Becton Dickinson) Annexin V-PE is a sensitive probe used to identify apoptotic cells. It binds to negatively charged phospholipid surfaces, with a higher specificity for phosphatidylserine (PS) than other phospholipids. Purified recombinant Annexin V was conjugated to phycoerythrin (PE). Annexin V-PE is routinely used to characterize primary cells or cell lines undergoing apoptosis. RevertAid First Strand cDNA Synthesis kit and QuantiNova SYBR Green PCR Kit (Thermo Scientific). Chromogenic agents (Invitrogen, USA). Chemiluminescence western blot detection kit (Thermo Scientific). Anti-GAPDH, anti-mTOR, anti-LC3, anti-Beclin 1, anti-BCL-2, anti-BCL-XL, anti-TMEM-49, anti-SQSTM-1/P62, and anti-α-SMA (Abcam Co, UK).

2.2. Cell culture

LX-2 cells (Punosai Life Technology Co. Wuhan China) were cultured at 37°C in 5% CO_2 and 95% air at 100% humidity in Dulbecco's Modified Eagle's Medium (DMEM) plus 10% heat-inactivated FBS, 100 mg mL^{-1} penicillin, and 100 mg mL^{-1} streptomycin (Thermo Scientific). Cell media was changed once every two days. When cells reached 80–90% confluence, they were trypsinized in 0.25% trypsin and passaged into 6-well plates for iAs trioxide exposure.

2.3. Cell treatments and groups

LX-2 cells were seeded into 96-well plates at 5,000 cells per well. iAs^{3+} were added at different concentrations when cell confluence reached 60% (Table 1).

Table 1
Cell groups

Group	Arsenic concentration
high iAs^{3+}group	5.00 μmol/L
middle iAs^{3+} group	0.50 μmol/L
low iAs^{3+} group	0.05 μmol/L
control group	0.00 μmol/L
infected only group	0.00 μmol/L

2.4. Cell infections

Before infection, LX-2 cells were resuspended at 1×10^5/mL in 6-well plates for 16–24 h. The first well was the control (cells only). The virus was defrosted and diluted in cold PBS to 1×10^7 TU/mL (MOI = 10) (TU/mL = number of bioactive virus particles per mL and MOI = multiplicity of infection). Virus was added to cells after 8–12 h, with growth in complete medium up to 72 h. Then, 2 μg/mL puromycin was added to wells and cultures maintained for 3–5 days, until all control cells died, At this point, live cells in remaining wells were assumed to be stably transfected with RFP-GFP-LC3. The medium was replaced with medium plus 0.5 μg/mL puromycin until cell fusion reached approximately 80%. At this point, cells were digested with pancreatic enzymes to ensure stable infection. At 14 days, cells were collected and assumed to be fully stable cell lines. RFP and GFP signals were observed using fluorescence microscopy (Borris Technologies, Co. Beijing, China). RFP was used to tag and track LC3, whereas weakened GFP indicated lysosome and autophagosome fusion to form autophagosomes/lysosomes. Fluorescence infection rates were detected by flow cytometry.

2.5. Apoptosis determination using flow cytometry

Flow cytometry (Bio-RAD,America)was used to analyze cell death processes. The Annexin V-fluorescein isothiocyanate (V-FITC) apoptosis detection kit (BioVision, USA) was used according to manufacturer's instructions. When the cell density reached 70–80%, the old medium was removed and different sodium arsenite concentrations in new medium added for 48 h. Cells were then harvested, washed in 1 × phosphate buffered saline (PBS; pH 7.4–7.5), and suspended in 500 μL 1 × Annexin V binding buffe. To this, 5 μL Annexin V-FITC and 5 μL propidium iodide (PI) (Trevigen ,America)were added and cells incubated for 5 min in the dark. Finally, cells were processed by flow cytometry.

2.6. Quantitative real-time PCR (qRT-PCR analysis)

Total RNA was isolated from LX-2 cells using the RNAiso kit (Takara, China) following manufacturer’s instructions. Total RNA was reverse-transcribed to cDNA using the Primer Script™ RT Master Mix kit (Takara Bio, Beijing, China). Then, qRT-PCR was performed using the SYBR ® Premix Ex Taq™II (2×) mix (Takara Bio) using a CFX 96-type RT fluorescence quantitative PCR instrument (Bio-Rad, USA). GAPDH

was used as a reference gene. Cycle thresholds were determined for each sample and each gene amplification. Based on the $2^{-\Delta\Delta Ct}$ method, relative target gene expression was calculated. Primer sequences are shown (Table 2).

Table 2
Primers for quantitative real-time PCR

Gene	Forward (5′–3′)	Reverse (3′–5′)
LC3	AAGGCGCTTACAGCTCAATG	CTGGGAGGCATAGACCATGT
Beclin-1	CCATGCAGGTGAGCTTCGT	GAATCTGCGAGAGACACCATC
SQSTM-1/P62	GCACCCCAATGTGATCTGC	CGCTACACAAGTAGTCTGG
BCL-2	GGTGGGGTCATGTGTGTGG	CGGTTCAGGTACTCAGTCATCC
BCL-XL	GAGCTGGTTGACTTTCTC	TCCATCTCCGATTCAGTCCCT
ATG4	ACCAGAGTAAGGGCACCTCT	CCTCCTAATGCCCAAGACTG
ATG5	CGAGATGTGTGGTTTGGACGA	AATGCCATTTCAGTGGTGTGC
ATG8	GGCTCCCAAAGCTCGGATAG	TACAGCTGACCCATTGTGGC
GAPDH	CACCCACTCCTCCACCTTTG	CCACCACCCTGTTGCTGTAG

Note: LC3; microtubule-associated protein light chain A/B; Beclin-1; recombinant human autophagy effector protein; SQSTM-1/P62; ubiquitin binding protein; BCL-2; B cell lymphoma-2; BCL-XL; recombinant human B-cell leukemia/lymphoma-2 XL; ATG4; autophagy related 4; ATG5; autophagy related 5; ATG8; autophagy related 8; GAPDH; glyceraldehyde-3-phosphate dehydrogenase

2.7. Western blotting

After treatments, total protein was extracted using ice-cold RIPA lysis buffer (plus phenylmethylsulfonyl fluoride) and concentrations determined by bicinchoninic acid assay (BCA) protein quantification kit (Thermo Scientific). Protein samples (30 μg) were separated using 6%, 10% or 12.5% sodium dodecyl sulfate-polyacrylamide gel electrophoresis, with proteins transferred to 0.22-μm polyvinylidene fluoride membranes (Sangon Biotech, Shanghai, China). After blocking in 5% skimmed milk for 1 h at 37°C, blots were incubated with primary antibodies; LC3 antibody (dilution 1:1000), Beclin-1 (dilution 1:2000), SQSTM-1/P62 (dilution 1:1000), BCL-2 (dilution 1:500), and GAPDH (dilution 1:10000) overnight at 4°C. Then blots were rinsed three times with Tween (Sangon Biotech) plus PBS and incubated with horseradish peroxidase (HRP)-conjugated secondary antibodies (Sangon Biotech) (1:8000) for 1 h. Immunoreactivity was visualized using an alkaline phosphatase color development kit (Sangon Biotech). Image analysis software ImageJ v1.51 (National Institutes of Health, USA) was used to calculate relative protein expression.

2.8. GFP and RFP fluorescence analysis

Cell lines infected for 14 days were harvested and cultured in confocal dishes (Sangon Biotech). Each dish was incubated with different $NaAsO_2$ and 3-MA concentrations for 48 h. 3-MA is an autophagy pathway inhibitor and was used to assess whether $NaAsO_2$ affected LX-2 autophagy. All subsequent arsenic cell assays were based on autophagy under fluorescence after transfection. A laser confocal microscope was used to capture GFP and RFP signals.

2.9. Statistical analysis

All experiments were performed at least 3 times. All data were represented as the mean ± standard error of the mean (SEM). Statistically significant differences between groups were analyzed using a single-factor analysis of variance (ANOVA) followed by two sided Student's t-test in the SPSS.22.0. P values < 0.05 were considered statistically significant.

3. Results

3.1. The effects of $NaAsO_2$ on LX-2 morphology

LX-2 cells in the blank group grew well after 24 h; cells were fusiform or star-shaped, with clear boundaries (Figure 1a). In high dose iAs^{3+} groups after 24 h, cell numbers decreased with culture time and cell morphology had changed: cells were no longer stretched but were more circular in morphology (Figure 1b).LX-2 cells in In high dose iAs^{3+} groups after 72h, cell lost original morphology, and cell numbers decreased dramatically (Figure 1c).

3.2. Autophagy observations

RFP-GFP-LC3 punctae in RFP-GFP-LC3-LX-2 cells were detected using laser confocal microscopy: in the control group, RFP-GFP-LC3 punctae were uniformly distributed in the cytoplasm (Figure 2a, b). Autophagosome/lysosome fusion is shown (Figure 2c). After serum-free medium was added to induce starvation, red and green fluorescent punctae were increased, with red fluorescence more abundant than green. (Figure 2d, e), indicating autophagy. In Figure 2F, yellow fluorescence represented autophagy and red represented autophagic lysosomes, thus starvation conditions had induced autophagy. In the absence of drugs, hunger-induced autophagy was observed under fluorescence, indicating the successful construction of an autophagy model using lentiviral RFP-GFP-LC3.

3.3. The effects of $NaAsO_2$ on early apoptotic rates in LX-2 cells stably expressing RFP-GFP-LC3

When compared with the blank (apoptotic rate = 2.35% ± 0.07%) and infected group (apoptotic rate = 2.15% ± 0.07%), the apoptotic rate in the infected + low iAs^{3+} group was 8.35% ± 0.64%, infected + medium iAs^{3+}group, 15.95% ± 1.48%, and 23.70% ± 0.85% in the infected + high iAs^{3+}group. Thus, as arsenic concentrations increased, apoptosis rates increased in a dose-dependent manner. Apoptosis rates between groups were statistically significant (P < 0.05) (Table 3 and Figure 3).

Table 3

The effects of $NaAsO_2$ on apoptotic rates in LX-2 cells after lentivirus infection ($\bar{x} \pm s$ %, n = 3).

Group	Apoptosis rate (%)
Control group	2.35 ± 0.07
infected only group	2.15 ± 0.07
Infected + low iAs^{3+}	8.35 ± 0.64*
Infected + medium iAs^{3+}	15.95 ± 1.48*
Infected + high iAs^{3+}	23.70 ± 0.85*
Note: n = 3 represents the same cell, and the same treatment was repeated three times; * indicates statistically significant differences when compared with the blank group.	

3.4. The effects of $NaAsO_2$ on LC3, Beclin-1, ATG4, ATG5, and ATG8 mRNA expression in LX-2 cells stably expressing RFP-GFP-LC3

To determine whether iAs^{3+} induced autophagy, we examined LC3, Beclin-1, ATG4, ATG5, and ATG8 expression levels in LX-2 cells after exposure to $NaAsO_2$.

The effects of iAs^{3+} on LC3, Beclin-1, ATG4, ATG5, and ATG8 mRNA expression in LX-2 cells after lentivirus infection are shown (Table 4). When we compared the blank and infection alone group, LC3 mRNA expression was significantly increased in the infection alone group. Thus, to better characterize autophagy, our transfection model may have also impacted other autophagy-related genes, thus after qRT-PCR, we used the transfection group as another control group. Similar to LC3, Beclin-1, ATG4, and ATG5 mRNA expression levels increased in infection groups. ATG8 mRNA was unaffected by transfection.

Table 4
The effects of $NaAsO_2$ on LC3, Beclin-1, ATG4, ATG5, and ATG8 mRNA expression in LX-2 cells after lentivirus infection ($\bar{x} \pm s$ n = 3).

Group	LC3	Beclin-1	ATG4	ATG5	ATG8
Blank group	1.25 ± 0.21	1.10 ± 0.53	1.13 ± 0.63	1.00 ± 0.04	1.01 ± 0.15
Infection group	20.09 ± 6.50[a]	22.46 ± 0.66[a]	2.38 ± 0.48[a]	2.26 ± 0.25[a]	1.43 ± 0.15
Infected + high As^{3+}	36.57 ± 9.68[ab]	13.38 ± 2.27[a]	3.39 ± 0.17[a]	1.65 ± 0.15[ab]	1.75 ± 0.08[a]
Infected + medium iAs^{3+}	4.14 ± 0.00[bc]	20.80 ± 6.95[a]	4.67 ± 1.38[ab]	2.62 ± 0.42[ac]	2.89 ± 0.61[abc]
Infected + low iAs^{3+}	14.19 ± 6.17[ac]	24.31 ± 7.09[ac]	5.23 ± 0.64[abc]	2.56 ± 0.21[ac]	2.34 ± 0.55[ab]
F	17.45	11.29	17.64	26.97	11.52
P	0.00	0.00	0.00	0.00	0.00

Note: compared with blank group, [a]$p < 0.05$; compared with infection group, [b]$p < 0.05$; compared with infected + high iAs^{3+}, [c]$p < 0.05$.

In all transfection groups, LC3 mRNA expression levels tended to initially decrease, then increase with increasing As^{3+} doses (infected + low iAs^{3+}: 14.19 ± 6.17; infected + medium iAs^{3+}: 4.14 ± 0.00; infected + high As^{3+}: 36.57 ± 9.68, $p < 0.05$) (Table 4).

Beclin-1 mRNA expression levels tended to decrease with increased iAs^{3+} dose (infected + low iAs^{3+}: 24.31 ± 7.09; infected + medium iAs^{3+}: 20.80 ± 6.95; infected + high As^{3+}: 13.38 ± 2.27, $p < 0.05$). ATG4, ATG5, and ATG8 mRNA expression levels tended to initially increase, then decrease with increased iAs^{3+} dose ($p < 0.05$) (Table 4).

3.5. The effects of $NaAsO_2$ on BCL-2 and BCL-XL mRNA expression in LX-2 cells stably expressing RFP-GFP-LC3

To confirm iAs^{3+} induced apoptosis and to identify a relationship between autophagy and apoptosis, we investigated expression of the apoptosis-related genes, BCL-2 and BCL-XL in LX-2 cells after treatments. When compared with the blank and infection alone group (these groups exhibited no apoptosis-related gene expression differences when infected), BCL-2 mRNA levels in infected + high and medium iAs^{3+} groups were increased. BCL-XL mRNA levels were decreased in the infected + high iAs^{3+} group ($p < 0.05$) (Table 5).

Table 5
The effects of $NaAsO_2$ on BCL-2 and BCL-XL mRNA expression in LX-2 cells after lentivirus infection ($\bar{x} \pm s$ n = 3).

Group	BCL-2	BCL-XL
Blank group	0.75 ± 0.35	1.04 ± 0.24
Infection group	0.78 ± 0.22	1.12 ± 0.18
Infected + high iAs^{3+}	6.93 ± 1.53^{ab}	0.52 ± 0.21^{ab}
Infected + medium iAs^{3+}	2.81 ± 0.82^{abc}	0.71 ± 0.17^{b}
Infected+ low iAs^{3+}	1.33 ± 0.34^{c}	0.81 ± 0.18
F	27.18	4.67
P	0.00	0.00

Note: compared with blank group, $^{a}p < 0.05$; compared with the infection group, $^{b}p < 0.05$; compared with infected + high iAs^{3+} group, $^{c}p < 0.05$; compared with infected + medium iAs^{3+} group, $^{d}p < 0.05$.

3.6. The effects of $NaAsO_2$ on LC3, Beclin-1, SQSTM-1/P62, TMEM-49, and mTOR protein expression in LX-2 cells

To further confirm autophagosome accumulation and apoptosis induced by arsenic, the translational levels of the autophagic markers, LC3, Beclin-1, SQSTM-1/P62, and TMEM-49, and the apoptosis marker, mTOR were examined in LX-2 cells by western blotting.

The effects of iAs^{3+} on LC3, Beclin-1, SQSTM-1/P62, TMEM-49, and mTOR protein expression in LX-2 cells after lentivirus infection were analyzed. When we compared the blank with the infection alone group, LC3 and Beclin-1 expression levels were both significantly increased. SQSTM-1/P62, TMEM-49, and mTOR levels were unaffected.

In all infection groups, when compared with the infection alone group, LC3 and mTOR expression levels tended to decrease in a dose-dependent manner. Beclin-1, SQSTM-1/P62, and TMEM-49 expression levels tended to increase first, then decrease with increased iAs^{3+} dose ($p < 0.05$) (Table 6, Figure 4).

Table 6

The effect of $NaAsO_2$ on LC3, Beclin-1, SQSTM-1/P62, TMEM-49, and mTOR expression in LX-2 cells ($\bar{x} \pm s$, n = 3).

Group	LC3	Beclin-1	SQSTM-1/P62	TMEM-49	mTOR
Blank group	0.04 ± 0.01	0.25 ± 0.01	0.21 ± 0.06	0.37 ± 0.03	0.81 ± 0.02
Infection group	0.20 ± 0.06[a]	0.53 ± 0.03	0.20 ± 0.06	0.37 ± 0.01	0.93 ± 0.02
Infected + high iAs^{3+}	0.09 ± 0.01[b]	0.44 ± 0.05	0.24 ± 0.07	0.42 ± 0.02	0.57 ± 0.11[ab]
Infected + medium iAs^{3+}	0.15 ± 0.00[a]	0.83 ± 0.03[a]	0.37 ± 0.04[ab]	0.58 ± 0.03[abc]	0.47 ± 0.07[ab]
Infected+ low iAs^{3+}	0.16 ± 0.0[ac]	1.20 ± 0.02[abc]	0.45 ± 0.01[abc]	0.49 ± 0.00[abcd]	0.50 ± 0.08[ab]
F	11.08	11.75	8.31	30.40	17.18
P	0.00	0.00	0.00	0.00	0.00

Note: compared with blank group, [a]$p < 0.05$; compared with infection group, [b]$p < 0.05$; compared with infected + high iAs^{3+} group, [c]$p < 0.05$; compared with infected + medium iAs^{3+}group, [d]$p < 0.05$.

3.7. The effects of $NaAsO_2$ on BCL-2 and BCL-XL protein expression in LX-2 cells

The effects of iAs^{3+} on BCL-2 and BCL-XL protein expression in LX-2 cells after lentivirus infection were also investigated. When we compared the blank with the infection alone group, BCL-XL levels were increased and BCL-2 levels unaffected. In all infection groups, when compared with the infection alone group, BCL-XL levels were first decreased, then increased with increasing iAs^{3+} dose ($p < 0.05$). BCL-2 levels were increased significantly in a dose dependent manner ($p < 0.05$) (Table 7, Figure 5).

Table 7
The effects of sodium arsenite on BCL-2 and BCL-XL expression in LX-2 cells after lentivirus infection ($\bar{x} \pm s$, n = 3)

Group	BCL-2	BCL-XL
Blank group	0.30 ± 0.01	0.43 ± 0.01
Infection group	0.28 ± 0.07	0.56 ± 0.03[a]
Infected + high iAs^{3+}	1.30 ± 0.01[ab]	0.84 ± 0.05[ab]
Infected + medium iAs^{3+}	0.90 ± 0.01[abc]	0.53 ± 0.03[ac]
Infected+ low iAs^{3+}	0.82 ± 0.01[abc]	0.38 ± 0.00[bcd]
F	22.25	61.74
P	0.00	0.00

Note: compared with blank group, [a]$p < 0.05$; compared with infection group, [b]$p < 0.05$; compared with infected + high iAs^{3+} group, [c]$p < 0.05$; compared with infected + medium iAs^{3+}group, [d]$p < 0.05$.

3.8. The effects of $NaAsO_2$ on α-SMA expression in LX-2 cells stably expressing RFP-GFP-LC3

To clarify if arsenic-induced autophagy was related to fibrosis, we assessed α-SMA expression in LX-2 cells after lentivirus infection. When we compared the blank with the infection alone group, α-SMA level were unaffected by infection. In all iAs^{3+} infection groups, when compared with the infection alone group, α-SMA levels were upregulated ($p < 0.05$) (Table 8, Figure 6).

Table 8
The effects of sodium arsenite on α-SMA expression in LX-2 cells after lentivirus infection ($\bar{x} \pm s$, n = 3)

Group	α-SMA
Blank group	0.40 ± 0.07
Infection group	0.48 ± 0.04
Infected + high iAs^{3+}	0.62 ± 0.01^{a}
Infected + medium iAs^{3+}	0.78 ± 0.10^{abc}
Infected + low iAs^{3+}	0.68 ± 0.06^{ab}
F	12.13
P	0.00

Note: compared with blank group, $^{a}p < 0.05$; compared with the infection group, $^{b}p < 0.05$; compared with infected + high iAs^{3+} group, $^{c}p < 0.05$; compared with infected + medium iAs^{3+}group, $^{d}p < 0.05$.

3.9. The effects of the autophagy inhibitor, 3-MA combined with $NaAsO_2$ on LC3, Beclin-1, and SQSTM-1/P62 mRNA levels in LX-2 cells stably expressing RFP-GFP-LC3

3-MA is an autophagy inhibitor and was used to evaluate arsenic-induced autophagy in LX-2 cells. Our data showed that except for the infected group, LC3 mRNA expression increased in all dose groups. Beclin-1 expression increased in the high dose trivalent arsenic, trivalent MA groups. SQSTM-1/P62 expression increased in trivalent arsenic high dose groups($p < 0.05$). Beclin-1 expression levels increased in the trivalent arsenic high dose group and the 3-MA trivalent arsenic high dose group. SQSTM-1/P62 expression levels were upregulated in the trivalent high dose groups ($p < 0.05$). When compared to the 3-MA group, LC3 expression in the high dose 3-MA trivalent group was upregulated (Table 9).

Table 9
The effects of 3-MA combined with $NaAsO_2$ on LC3, Beclin-1, and SQSTM-1/P62 mRNA expression levels in LX-2 cells after lentivirus infection ($\bar{x}\pm s$, n = 3).

Group	LC3	Beclin-1	SQSTM-1/P62
Blank group	1.00±0.57	1.05±0.37	1.08±0.48
Infection group	3.59±0.30	1.68±0.96	2.12±0.04
3-MA group	8.49 ± 0.48^{ab}	5.68 ± 0.59^{ab}	4.93 ± 0.31^{a}
Infected + high iAs^{3+}	36.57 ± 8.25^{abc}	8.29 ± 1.20^{abc}	2.17 ± 0.04^{c}
3-MA + high iAs^{3+}	9.51 ± 0.57^{ab}	11.20 ± 0.44^{abc}	11.64 ± 4.57^{abc}
F	102.98	265.08	28.13
P	0.00	0.00	0.00

Note: Compared with blank group, $^{a}P < 0.05$; compared to the infection group, $^{b}p < 0.05$; compared to the 3-MA group, $^{c}p < 0.05$.

3.10. The effects of 3-MA combined with $NaAsO_2$ on LC3, Beclin-1, and SQSTM-1/P62 expression in in LX-2 cells stably expressing RFP-GFP-LC3

When compared with the blank group, LC3 levels were increased in each dose group except the infected group. Higher Beclin-1 levels were observed in the high iAs^{3+}, 3-MA + high iAs^{3+} groups. SQSTM-1/P62 levels were increased in in high iAs^{3+}group ($p < 0.05$).

When compared to the 3-MA group, elevated LC3 levels were observed in 3-MA + high iAs^{3+} group. Beclin-1 levels were increased in high iAs^{3+} and 3-MA + high iAs^{3+} groups. SQSTM-1/P62 levels were also elevated in 3-MA + high iAs^{3+} ($p < 0.05$) (Table 10, Figure 7).

Table 10
The effects of 3-MA combined with $NaAsO_2$ on LC3, Beclin-1, and SQSTM-1/P62 protein expression levels in LX-2 cells after lentivirus infection ($\bar{x} \pm s$, n = 3).

Group	LC3	Beclin-1	SQSTM-1/P62
Blank group	0.29 ± 0.01	0.84 ± 0.07	0.75 ± 0.04
Infection group	0.38 ± 0.00	0.81 ± 0.03	0.83 ± 0.05
3-MA group	0.81 ± 0.06^{ab}	0.95 ± 0.04	0.74 ± 0.02^{b}
Infected + high iAs^{3+}	1.01 ± 0.02^{ab}	1.25 ± 0.03^{abc}	0.96 ± 0.03^{abc}
3-MA + high iAs^{3+}	1.49 ± 0.29^{abc}	1.41 ± 0.12^{abc}	0.83 ± 0.02^{c}
F	27.80	29.59	14.69
P	0.00	0.00	0.01

Note: Compared with blank group, $^{a}P < 0.05$; compared to the infection group, $^{b}p < 0.05$; compared to the 3-MA group, $^{c}p < 0.05$.

4. Discussion

4.1. LX-2 cell lines stably expressing RFP-GFP-LC3 lentivirus vectors contribute to autophagy observations

In recent years, autophagy has been associated with key roles in several human diseases[29]. Increasingly, studies have confirmed autophagy maintains cellular and tissue homeostasis by regulating various physiological processes, including cytokine formation, pathogen clearance, antigen presentation, inflammatory responses, and innate and adaptive immune responses[30]. Autophagy is a complex multi-step process, comprising initiation, nucleation, extension and closure, and lysosomal fusion[31]. Thus, the accurate dissection of autophagy is crucial for studying autophagic biological functions. In our study, we constructed an autophagic bi-functional lentiviral RFP-GFP-LC3 vector for stable transfection into cell lines. The molecular premise was that red and green punctae would represent autophagic mechanisms. Thus, characteristic autophagosomes could be fluorescently displayed at different stages in the autophagy pathway. The establishment of stable cell lines expressing RFP-GFP-LC3 provided a reliable cellular platform for detecting and assessing autophagic flux. Our approach was highly beneficial for studying the autophagic effects of arsenic-induced HSCs and lays the foundation for the identification of mechanisms underpinning arsenic induced liver fibrosis.

4.2. The effects of $NaAsO_2$ on autophagy levels in LX-2 cells

The liver is an important detoxification organ and is vulnerable when processing poisonous substances[32]. During hepatic fibrosis, HSCs invade target cells due to a variety of external factors, transforming them into myofibroblasts. α-SMA is present only in the liver and in large vascular smooth muscle. When HSCs are stationary, they do not express α-SMA, exhibit low proliferative activity, and low synthetic collagen capabilities. However, when the liver is damaged via inflammation or mechanical stimulation, HSCs activate and transform into myofibroblast-like cells, and express α-SMA[33] which is an important marker of HSC activation. Inorganic As causes liver injury, especially liver fibrosis[34]. Tao *et al.* observed that chronic $NaAsO_2$ ingestion caused liver fibrosis and oxidative stress in Sprague-Dawley rats, along with collagen deposition, and HSC activation[21]. In our study, in LX-2 cell lines induced by iAs^{3+} for 48 h, α-SMA expression increased significantly, suggesting iAs^{3+} induced HSC activation *in vitro*, consistent with previous findings. Thus, an *in vitro* HSC induced iAs^{3+} model was successfully established.

Autophagy activity and biological functions are regulated by several ATGs and associated proteins, including LC3, SQSTM-1/P62, Beclin-1, ATG4, ATG5, ATG8, and ATG12[35]. LC3 is involved in the formation of autophagy lysosomes and dissociates from lysosomal structures to digest damaged materials. P62 is a marker of autophagic flux which combines autophagy substrates with autophagy lysosomes for degradation[36]. Therefore, LC3 and P62 are typical autophagy biomarkers. Wu *et al.* reported that arsenic induced autophagy in pancreatic islets was evidenced by elevated LC3-II levels and depressed P62 levels, both in vivo and in vitro[37]. Based on our data, after trivalent and pentavalent arsenic treatment, LC3 mRNA expression levels were increased, and the highest increase was observed in the high trivalent arsenic dose group. In addition, the autophagy related gene, ATG5 strictly controls autophagy and plays a crucial role in autophagosome formation; previous studies have shown that ATG5 and ATG4 gene expression levels promote autophagy[38]. In our study, ATG4, ATG5, and ATG8 gene levels were upregulated in each iAs^{3+} dose group. Moreover, Beclin-1 is a key regulator of autophagy; it promotes the transformation of LC3-I to LC3-II, thereby reflecting autophagy activation[39]. Previous evidence has suggested mTOR is a regulatory autophagy inhibitor, promotes Beclin-1 release, and is an important regulator in anabolism and catabolism, cell growth, and proliferation[9]. Other studies reported that arsenite-treated cells depleted mTOR levels which in turn increased lysosomal activity and promoted autophagy via the formation of autophagy lysosomes[25]. Our data showed that with increased iAs^{3+} doses, Beclin-1 and MEM-49 protein expression levels were upregulated and mTOR expression downregulated.

Common effector proteins associated with apoptosis and autophagy include BCL-2 and BCL-XL, and ATG5 respectively[40]. BCL-2 and BCL-XL are well-characterized anti-apoptotic proteins and may be key factors in regulating autophagy; they inhibit Beclin-1 mediated autophagy by interacting with Beclin-1[41]. Studies have shown that the JNK-Bcl-2/Bcl-xL-Bax/Bak pathway mediates crosstalk between matrine-induced autophagy and apoptosis via interplay with Beclin-1 (matrine is an alkaloid extracted from *Sophora flavescens*)[42]. Therefore, BCL-2 and BCL-XL have key roles in apoptosis and autophagy

interactions. Beclin-1 also inhibits cell proliferation, as observed in several cancers, including, tongue squamous cell carcinoma[43], breast cancer[44], hepatocellular carcinoma[45], and colorectal cancer. Autophagy blocking also activated apoptotic pathways and eventually led to apoptosis and death. Li[46] reported that in Raji cells induced with As_2O_3, autophagy vacuoles were formed, increasing autophagy degradation via P62 substrates, accompanied by upregulated Beclin-1 and downregulated BCL-2 expression. Levine[47]observed that Beclin-1 combined with BCL-2/BCL-XL to form a constitutive BCL-2/BCL-XL-Beclin-1 complex which reduced Beclin-1 monomer inhibition of autophagy. Our data showed that Beclin-1 levels were increased and BCL-2/BCL-XL levels inhibited in a dose-dependent trivalent arsenic manner, suggesting that with increased Beclin-1 monomers, apoptosis and autophagy were activated. These results were consistent with our studies, suggesting iAs^{3+} induced autophagy via apoptosis pathways.

4.3. The effects of 3-MA on autophagy induced by $NaAsO_2$ in LX-2 cells

3-MA is a commonly used inhibitor of the autophagy pathway[48]. Reports have shown 3-MA inhibits phosphoinositide 3-kinase (PI3K) activity and blocks the formation of proautophagosomes, autophagosomes, and autophagic vacuoles[24]. In our study, the formation of red and yellow fluorescent punctae in the 3-MA + trivalent arsenic high dose group was significantly reduced, while green fluorescent spots were increased, suggesting high-dose sodium arsenite inhibited autophagosome formation and promoted autophagy. Hence, 3-MA may further inhibit iAs^{3+}-induced autophagy in LX-2 cells. Wang[49] reported that arsenic sulfide (AS_2S_2) induced autophagy in human osteosarcoma cells, with upregulated LC3 and Beclin-1 expression. Using 3-MA, the inhibitory effects of AS_2S_2 on cell viability may be enhanced. When Tris (1,3-dichloro-2-propyl) hydrochloride was used to induce SH-SY5Y cells, 3-MA reduced Beclin-1, LC3-II, and SQSTM1/P62 expression, and significantly promoted apoptosis.

In our study, Beclin-1 gene and protein expression in LX-2 cells were significantly upregulated in iAs^{3+} treatment and 3-MA + iAs^{3+} treatment groups, suggesting iAs^{3+} affected early-stage autophagy. Upregulated Beclin-1 was observed in the combined treatment group, further suggesting 3-MA exacerbated autophagic processes. LC3 mRNA and protein expression levels in trivalent group was increased and SQSTM-1/P62 protein expression levels increased suggesting autophagy turnover was inhibited. Therefore, arsenic affects autophagy formation. LC3 and SQSTM-1/P62 gene expression increased in the 3-MA combined iAs^{3+} group, suggesting this commination blocked downstream autophagic flow by inhibiting autophagosome degradation, consistent with our autophagosome distribution images.

This study successfully established an LX-2 cell line stably expressing RFP-GFP-LC3, thereby generating a robust cellular platform to perform autophagy studies. After different arsenite doses were used to induce LX-2 cells, apoptosis rates increased and the cell cycle was blocked in the G0–G1 phase thereby affecting cell replication and inducing apoptosis. Alpha-SMA levels were also significantly elevated suggesting

HSC activation and the formation of hepatic fibrosis.Arsenic-induced autophagy occurrence in LX-2 cells may be mediated through the apoptotic pathway.Finally, 3-Methyladenine is able to reduce autophagage levels and may inhibit liver fibrosis induced by inorganic arsenic. However, further *in vitro* and *in vivo* research is required to explore how the mTOR pathway regulates arsenic-induced autophagy.

Declarations

Funding

We acknowledge financial support from the National Natural Science Foundation of China, China 82160650 and Open topics of Microtrace Elements and Local Disease Key Laboratory of National Health Commission.

Acknowledgments

The authors are grateful to the National Natural Science Foundation of China (82160650) and Open topics of Microtrace Elements and Local Disease Key Laboratory of National Health Commission.

Data availability

Data from this study may be accessed upon reasonable request to the corresponding author.

Conflict of interest

The authors declare no conflict of interest.

Author contributions

Shunhua Wu designed the study. Yu Hui performed experiments. Fei Huang and Rishalaiti Tayier drafted the manuscript. Ang Li performed analyses and interpreted the data. All authors read and approved the final manuscript.

References

1. Chandio, T. A. *et al.* Fluoride and arsenic contamination in drinking water due to mining activities and its impact on local area population. *Environ Sci Pollut Res Int* **28**, 2355–2368, doi:10.1007/s11356-020-10575-9 (2021).
2. Minatel, B. C. *et al.* Environmental arsenic exposure: From genetic susceptibility to pathogenesis. *Environ Int* **112**, 183–197, doi:10.1016/j.envint.2017.12.017 (2018).
3. Loomis, D., Guha, N., Hall, A. L. & Straif, K. Identifying occupational carcinogens: an update from the IARC Monographs. *Occup Environ Med* **75**, 593–603, doi:10.1136/oemed-2017-104944 (2018).
4. Mao, J. *et al.* Possible differences in the mechanism of malignant transformation of HaCaT cells by arsenite and its dimethyl metabolites, particularly dimethylthioarsenics. *J Trace Elem Med Biol* **61**,

126544, doi:10.1016/j.jtemb.2020.126544 (2020).

5. Zhang, L., Huang, Y., Ling, J., Xiang, Y. & Zhuo, W. Screening of key genes and prediction of therapeutic agents in Arsenic-induced lung carcinoma. *Cancer Biomark* **25**, 351–360, doi:10.3233/cbm-182333 (2019).
6. Liu, R., Tabuchi, T., Kitamura, T., Miyashiro, I. & Sobue, T. Long-term observational study on 6223 survivors of arsenic poisoning due to contaminated milk powder during infancy. *Cancer Sci* **111**, 3873–3880, doi:10.1111/cas.14623 (2020).
7. Perry, A., Lynch, R. M., Rusyn, I. & Threadgill, D. W. Long-Term Combinatorial Exposure to Trichloroethylene and Inorganic Arsenic in Genetically Heterogeneous Mice Results in Renal Tubular Damage and Cancer-Associated Molecular Changes. *G3 (Bethesda)* **9**, 1729-1737, doi:10.1534/g3.119.400161 (2019).
8. Song, Y., Jin, D., Chen, J., Liang, W. & Liu, X. Effects of Arsenic (+3 Oxidation State) Methyltransferase Gene Polymorphisms and Expression on Bladder Cancer: Evidence from a Systematic Review, Meta-analysis and TCGA Dataset. *Toxicol Sci* **177**, 27–40, doi:10.1093/toxsci/kfaa087 (2020).
9. Chen, Q. Y. & Costa, M. PI3K/Akt/mTOR Signaling Pathway and the Biphasic Effect of Arsenic in Carcinogenesis. *Mol Pharmacol* **94**, 784–792, doi:10.1124/mol.118.112268 (2018).
10. Xu, Y. *et al.* Assessing the potential value of Rosa Roxburghii Tratt in arsenic-induced liver damage based on elemental imbalance and oxidative damage. *Environ Geochem Health* **43**, 1165–1175, doi:10.1007/s10653-020-00612-4 (2021).
11. Hu, Y., Xiao, T. & Zhang, A. Associations between and risks of trace elements related to skin and liver damage induced by arsenic from coal burning. *Ecotoxicol Environ Saf* **208**, 111719, doi:10.1016/j.ecoenv.2020.111719 (2021).
12. Xue, J. *et al.* miR-21-regulated M2 polarization of macrophage is involved in arsenicosis-induced hepatic fibrosis through the activation of hepatic stellate cells. *J Cell Physiol* **236**, 6025–6041, doi:10.1002/jcp.30288 (2021).
13. Fang, S. *et al.* Arsenic trioxide induces macrophage autophagy and atheroprotection by regulating ROS-dependent TFEB nuclear translocation and AKT/mTOR pathway. *Cell Death Dis* **12**, 88, doi:10.1038/s41419-020-03357-1 (2021).
14. Wu, L. *et al.* Autophagy mediates bronchial cell malignant transformation induced by chronic arsenic exposure via MEK/ERK1/2 pathway. *Toxicol Lett* **332**, 155–163, doi:10.1016/j.toxlet.2020.06.006 (2020).
15. Levine, B. & Kroemer, G. Biological Functions of Autophagy Genes: A Disease Perspective. *Cell* **176**, 11–42, doi:10.1016/j.cell.2018.09.048 (2019).
16. Zhang, N. & Zhao, Y. Other Molecular Mechanisms Regulating Autophagy. *Adv Exp Med Biol* **1206**, 261–271, doi:10.1007/978-981-15-0602-4_13 (2019).
17. Oshima, M., Seki, T., Kurauchi, Y., Hisatsune, A. & Katsuki, H. Reciprocal Regulation of Chaperone-Mediated Autophagy/Microautophagy and Exosome Release. *Biol Pharm Bull* **42**, 1394–1401, doi:10.1248/bpb.b19-00316 (2019).

18. Markaki, M. & Tavernarakis, N. Autophagy mechanisms and roles: recent advances and implications. *Febs j* **287**, 5024–5026, doi:10.1111/febs.15573 (2020).
19. Wang, M. *et al.* The expression characteristics and prognostic roles of autophagy-related genes in gastric cancer. *PeerJ* **9**, e10814, doi:10.7717/peerj.10814 (2021).
20. Al-Bari, M. A. A. & Xu, P. Molecular regulation of autophagy machinery by mTOR-dependent and -independent pathways. *Ann N Y Acad Sci* **1467**, 3–20, doi:10.1111/nyas.14305 (2020).
21. Tao, Y. *et al.* IRE1α/NOX4 signaling pathway mediates ROS-dependent activation of hepatic stellate cells in NaAsO(2) -induced liver fibrosis. *J Cell Physiol* **236**, 1469–1480, doi:10.1002/jcp.29952 (2021).
22. Allaire, M., Rautou, P. E., Codogno, P. & Lotersztajn, S. Autophagy in liver diseases: Time for translation? *J Hepatol* **70**, 985–998, doi:10.1016/j.jhep.2019.01.026 (2019).
23. Zhang, H. *et al.* More serious autophagy can be induced by ZnO nanoparticles than single-walled carbon nanotubes in rat tracheal epithelial cells. *Environ Toxicol* **36**, 238–248, doi:10.1002/tox.23029 (2021).
24. Petiot, A., Ogier-Denis, E., Blommaart, E. F., Meijer, A. J. & Codogno, P. Distinct classes of phosphatidylinositol 3'-kinases are involved in signaling pathways that control macroautophagy in HT-29 cells. *J Biol Chem* **275**, 992–998, doi:10.1074/jbc.275.2.992 (2000).
25. Wu, C. W., Lin, P. J., Tsai, J. S., Lin, C. Y. & Lin, L. Y. Arsenite-induced apoptosis can be attenuated via depletion of mTOR activity to restore autophagy. *Toxicol Res (Camb)* **8**, 101–111, doi:10.1039/c8tx00238j (2019).
26. Chicote, J., Yuste, V. J., Boix, J. & Ribas, J. Cell Death Triggered by the Autophagy Inhibitory Drug 3-Methyladenine in Growing Conditions Proceeds With DNA Damage. *Front Pharmacol* **11**, 580343, doi:10.3389/fphar.2020.580343 (2020).
27. Zhang, X. *et al.* Inhibition of autophagy by 3-methyladenine restricts murine cytomegalovirus replication. *J Med Virol* **93**, 5001–5016, doi:10.1002/jmv.26787 (2021).
28. Peng, Y., Huang, K., Shen, L., Tao, Y. Y. & Liu, C. H. Cultured Mycelium Cordyceps sinensis allevi¬ates CCl4-induced liver inflammation and fibrosis in mice by activating hepatic natural killer cells. *Acta Pharmacol Sin* **37**, 204–216, doi:10.1038/aps.2015.129 (2016).
29. Shang, D., Wang, L., Klionsky, D. J., Cheng, H. & Zhou, R. Sex differences in autophagy-mediated diseases: toward precision medicine. *Autophagy* **17**, 1065–1076, doi:10.1080/15548627.2020.1752511 (2021).
30. Jiang, X., Chen, C., Liu, Y., Zhang, P. & Zhang, Z. Critical role of cellular glutathione homeostasis for trivalent inorganic arsenite-induced oxidative damage in human bronchial epithelial cells. *Mutat Res Genet Toxicol Environ Mutagen* **770**, 35–45, doi:10.1016/j.mrgentox.2014.04.016 (2014).
31. Cheung, Y. W. S., Nam, S. E. & Yip, C. K. Recent Advances in Single-Particle Electron Microscopic Analysis of Autophagy Degradation Machinery. *Int J Mol Sci* **21**, doi:10.3390/ijms21218051 (2020).
32. Mega, A., Marzi, L., Kob, M., Piccin, A. & Floreani, A. Food and Nutrition in the Pathogenesis of Liver Damage. *Nutrients* **13**, doi:10.3390/nu13041326 (2021).

33. Zakaria, S. *et al.* Value of α-smooth muscle actin and glial fibrillary acidic protein in predicting early hepatic fibrosis in chronic hepatitis C virus infection. *Arch Med Sci* **6**, 356–365, doi:10.5114/aoms.2010.14255 (2010).
34. Wang, Z. *et al.* Taurine protected As(2)O(3)-induced the activation of hepatic stellate cells through inhibiting PPARα-autophagy pathway. *Chem Biol Interact* **300**, 123–130, doi:10.1016/j.cbi.2019.01.019 (2019).
35. Ganley, I. G., Wong, P. M., Gammoh, N. & Jiang, X. Distinct autophagosomal-lysosomal fusion mechanism revealed by thapsigargin-induced autophagy arrest. *Mol Cell* **42**, 731–743, doi:10.1016/j.molcel.2011.04.024 (2011).
36. Liu, X. *et al.* Regulation of FN1 degradation by the p62/SQSTM1-dependent autophagy-lysosome pathway in HNSCC. *Int J Oral Sci* **12**, 34, doi:10.1038/s41368-020-00101-5 (2020).
37. Wu, W. *et al.* Pancreatic islet-autonomous effect of arsenic on insulin secretion through endoplasmic reticulum stress-autophagy pathway. *Food Chem Toxicol* **111**, 19–26, doi:10.1016/j.fct.2017.10.043 (2018).
38. Kim, J. *et al.* Atg5-mediated autophagy controls apoptosis/anoikis via p53/Rb pathway in naked mole-rat fibroblasts. *Biochem Biophys Res Commun* **528**, 146–153, doi:10.1016/j.bbrc.2020.05.083 (2020).
39. Hu, Y. J., Zhong, J. T., Gong, L., Zhang, S. C. & Zhou, S. H. Autophagy-Related Beclin 1 and Head and Neck Cancers. *Onco Targets Ther* **13**, 6213–6227, doi:10.2147/ott.S256072 (2020).
40. Dalby, K. N., Tekedereli, I., Lopez-Berestein, G. & Ozpolat, B. Targeting the prodeath and prosurvival functions of autophagy as novel therapeutic strategies in cancer. *Autophagy* **6**, 322–329, doi:10.4161/auto.6.3.11625 (2010).
41. Zhou, F., Yang, Y. & Xing, D. Bcl-2 and Bcl-xL play important roles in the crosstalk between autophagy and apoptosis. *Febs j* **278**, 403–413, doi:10.1111/j.1742-4658.2010.07965.x (2011).
42. Yang, J. & Yao, S. JNK-Bcl-2/Bcl-xL-Bax/Bak Pathway Mediates the Crosstalk between Matrine-Induced Autophagy and Apoptosis via Interplay with Beclin 1. *Int J Mol Sci* **16**, 25744–25758, doi:10.3390/ijms161025744 (2015).
43. Hu, Z. *et al.* Decreased expression of Beclin–1 is significantly associated with a poor prognosis in oral tongue squamous cell carcinoma. *Mol Med Rep* **14**, 1567–1573, doi:10.3892/mmr.2016.5437 (2016).
44. Wang, N. & Feng, Y. Elaborating the role of natural products-induced autophagy in cancer treatment: achievements and artifacts in the state of the art. *Biomed Res Int* 2015, 934207, doi:10.1155/2015/934207 (2015).
45. Qiu, D. M. *et al.* The expression of beclin-1, an autophagic gene, in hepatocellular carcinoma associated with clinical pathological and prognostic significance. *BMC Cancer* **14**, 327, doi:10.1186/1471-2407-14-327 (2014).
46. Li, C. L. *et al.* Arsenic trioxide induces autophagy and antitumor effects in Burkitt's lymphoma Raji cells. *Oncol Rep* **32**, 1557–1563, doi:10.3892/or.2014.3369 (2014).

47. Levine, B., Sinha, S. & Kroemer, G. Bcl-2 family members: dual regulators of apoptosis and autophagy. *Autophagy* **4**, 600–606 (2008).
48. Zhang, J. *et al.* 3-MA Enhanced Chemosensitivity in Cisplatin Resistant Hypopharyngeal Squamous Carcinoma Cells via Inhibiting Beclin -1 Mediated Autophagy. *Curr Pharm Des* **27**, 996–1005, doi:10.2174/1381612826666201221150431 (2021).
49. Wang, G. *et al.* Arsenic sulfide induces apoptosis and autophagy through the activation of ROS/JNK and suppression of Akt/mTOR signaling pathways in osteosarcoma. *Free Radic Biol Med* **106**, 24–37, doi:10.1016/j.freeradbiomed.2017.02.015 (2017).

Figures

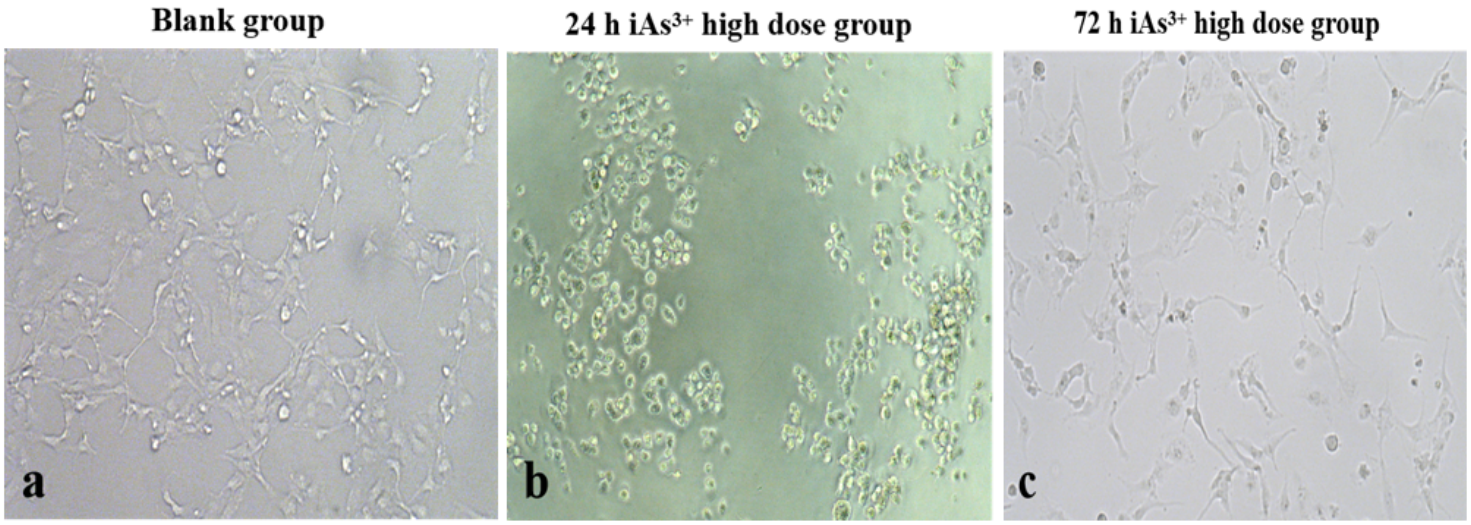

Figure 1

Morphological changes in LX-2 cells after iAs^{3+} exposure at different time intervals.

Note: (a) normal LX-2 cells after 24 h. Cells were fusiform or star-shaped, with clear boundaries. (b) 24 h iAs^{3+} high dose group exposure. (c) 72 h iAs^{3+} high dose group exposure.Cell numbers decreased with culture time, and the cells were no longer stretched but had become more circular

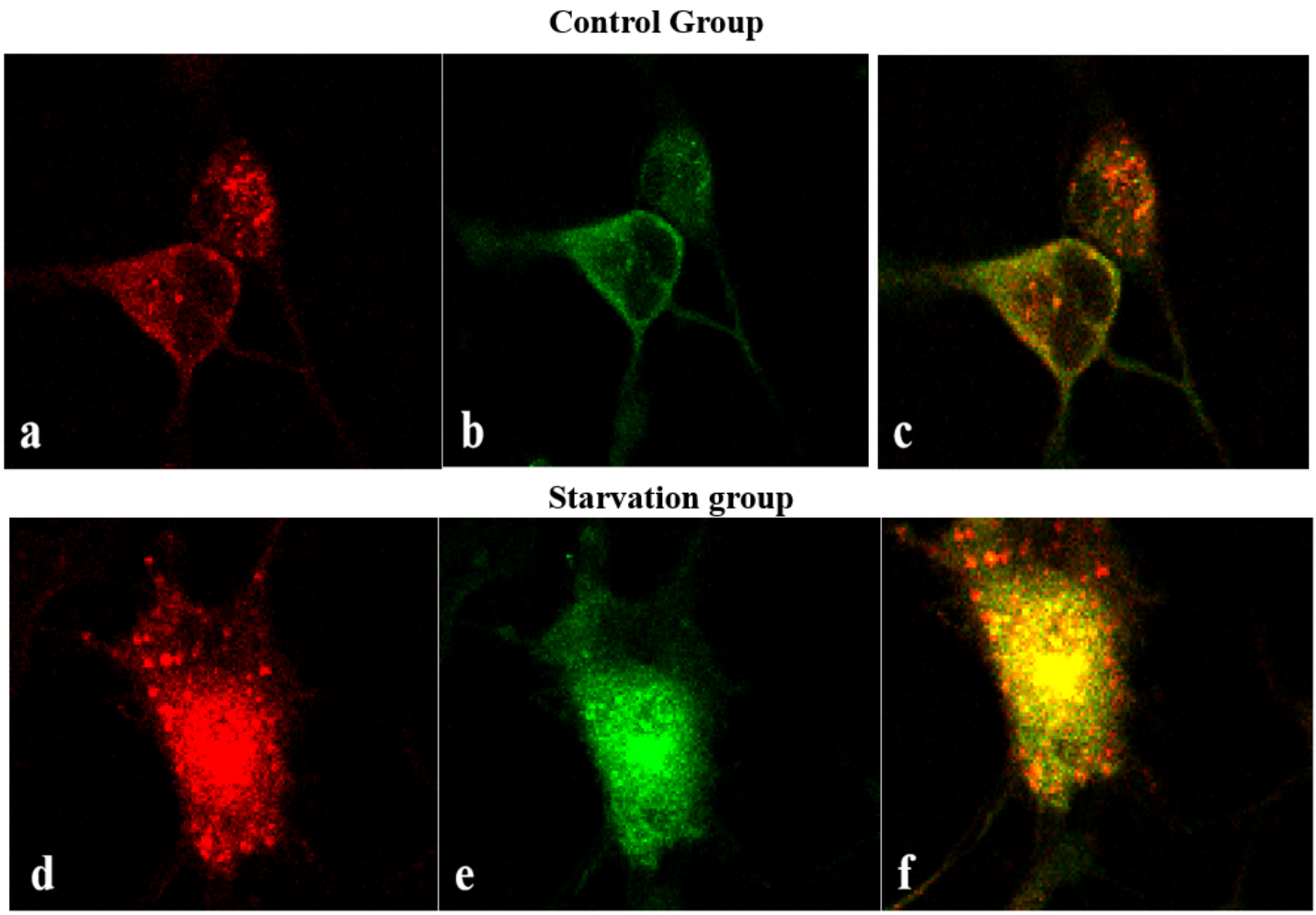

Figure 2

Autophagic punctae in RFP-GFP-LC3-LX-2 cells examined with fluorescence microscopy.

Note:Control group: a: red fluorescent autophagic punctae; b: green fluorescent autophagic punctae; c: a and b combined. Normal cultured cells are shown. RFP-GFP-LC3 spots are uniformly distributed in the cytoplasm. Starvation group: d: autophagic punctae under red fluorescence; e: autophagic punctae under green fluorescence;f: d and e combined. With serum-free medium added, both red and green fluorescent spots increased significantly, and more red spots than green spots were observed. The yellow spots formed after the fusion of green and red spots represent autophagosomes, and red spots represent autophagic lysosomes, thus indicating that hunger can induce autophagy, and the lysosome fusion path is unobstructed (Fig. F).

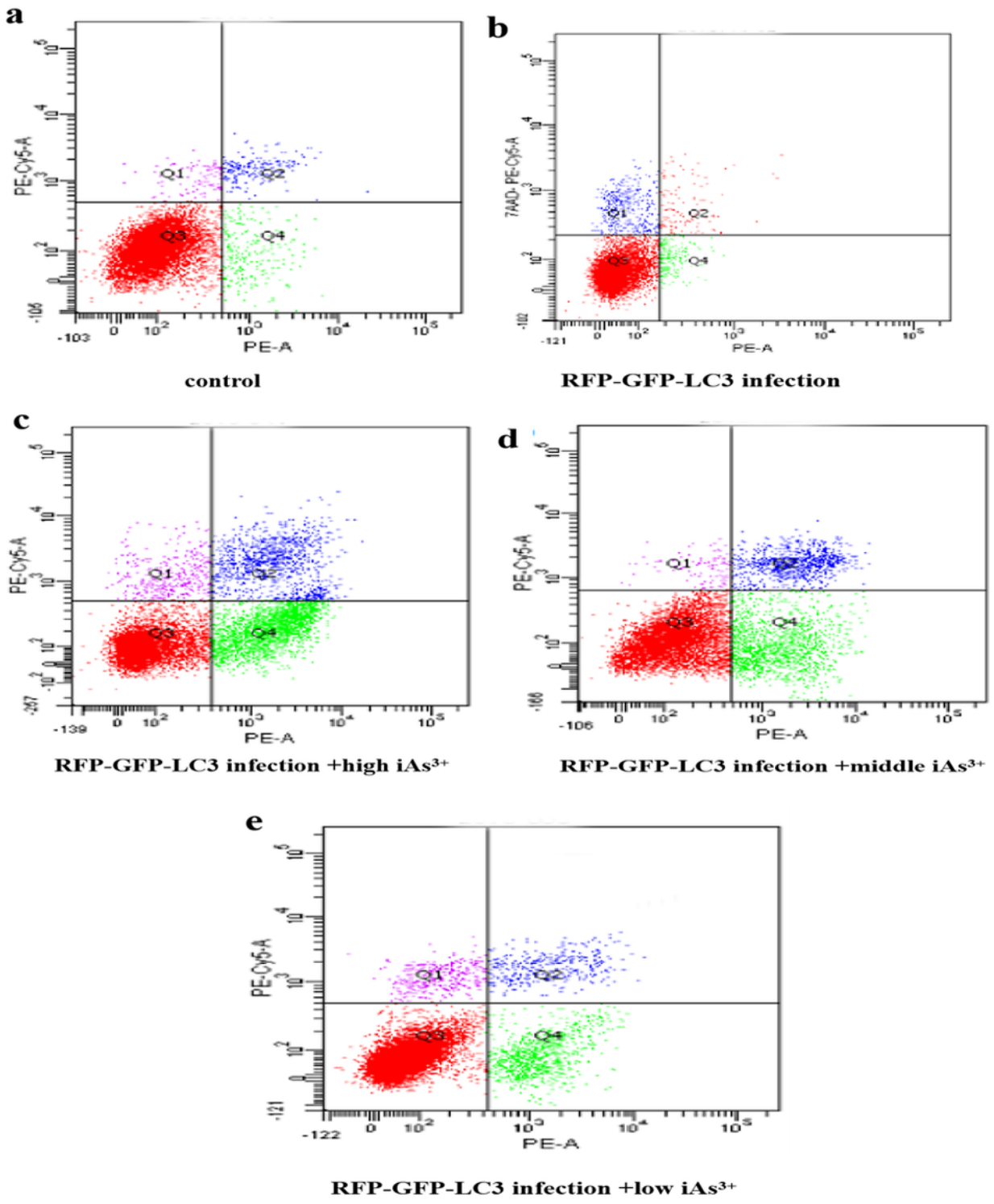

Figure 3

Apoptosis levels in LX-2 cell exposed to iAs^{3+}.

Note: a: Control group; b:FP-GFP-LC3 infected group; c:RFP-GFP-LC3 infected+high dose iAs^{3+} group; d:RFP-GFP-LC3 infected+middle iAs^{3+}group;e:RFP-GFP-LC3 infected+low iAs^{3+} group.Q4 quadrants represent apoptosis compared with blank and infection alone groups.The apoptosis rate was not

changed in Q4 regions.(Figure 3a,b) As arsenic concentrations increased, the apoptosis rate in a dose dependent manner in infected + iAs^{3+} (Figure 3c,d,e) .

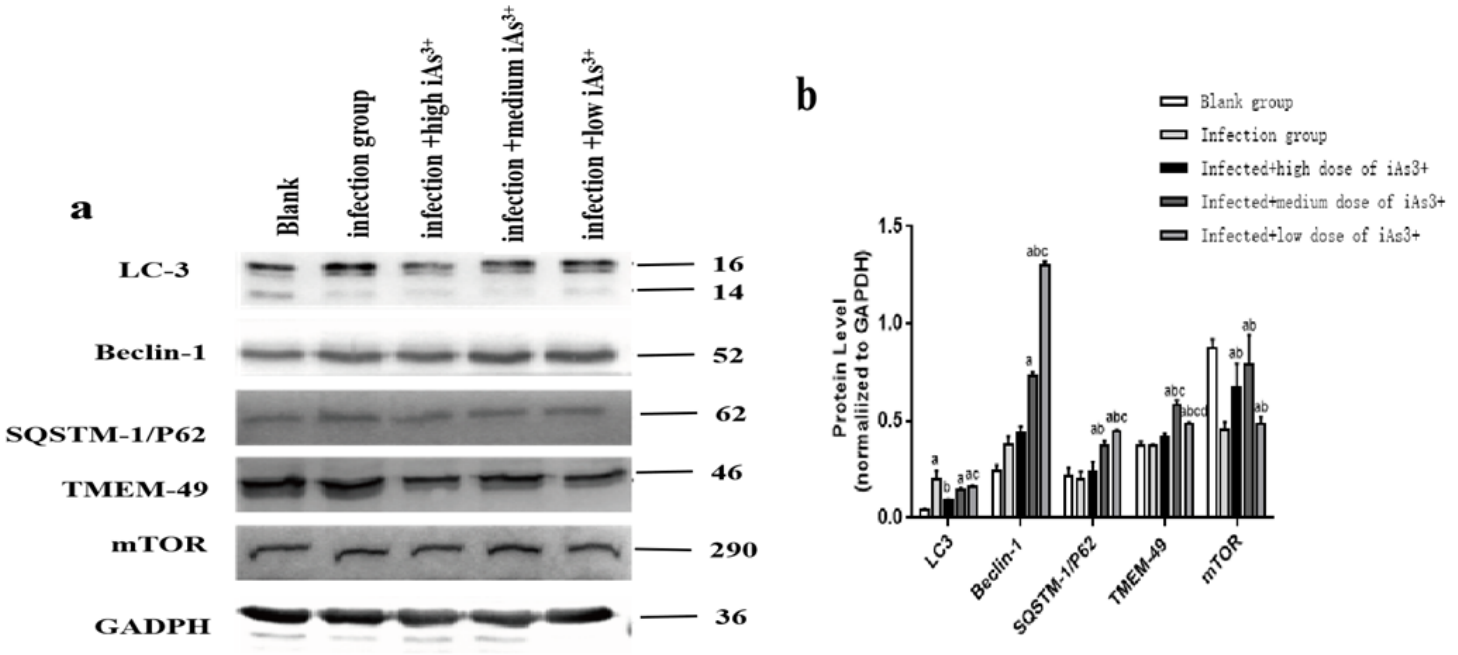

Figure 4

Western blot data for LC3, Beclin-1, SQSTM-1/P62, TMEM-49, and mTOR protein levels in LX-2 cells after iAs^{3+} treatment.

a) Molecular weight markers are shown on the right. b) The relative expression of LC3, Beclin-1, SQSTM-1/P62, TMEM-49, and mTOR proteins. (Note: different letters represent different comparisons. Compared with the blank group, $^{a}P < 0.05$; compared with the infected group, $^{b}P < 0.05$; Compared with the infection + high iAs^{3+} group, $^{c}P < 0.05$; and compared with the infection + medium iAs^{3+} dose group, $^{d}P < 0.05$.

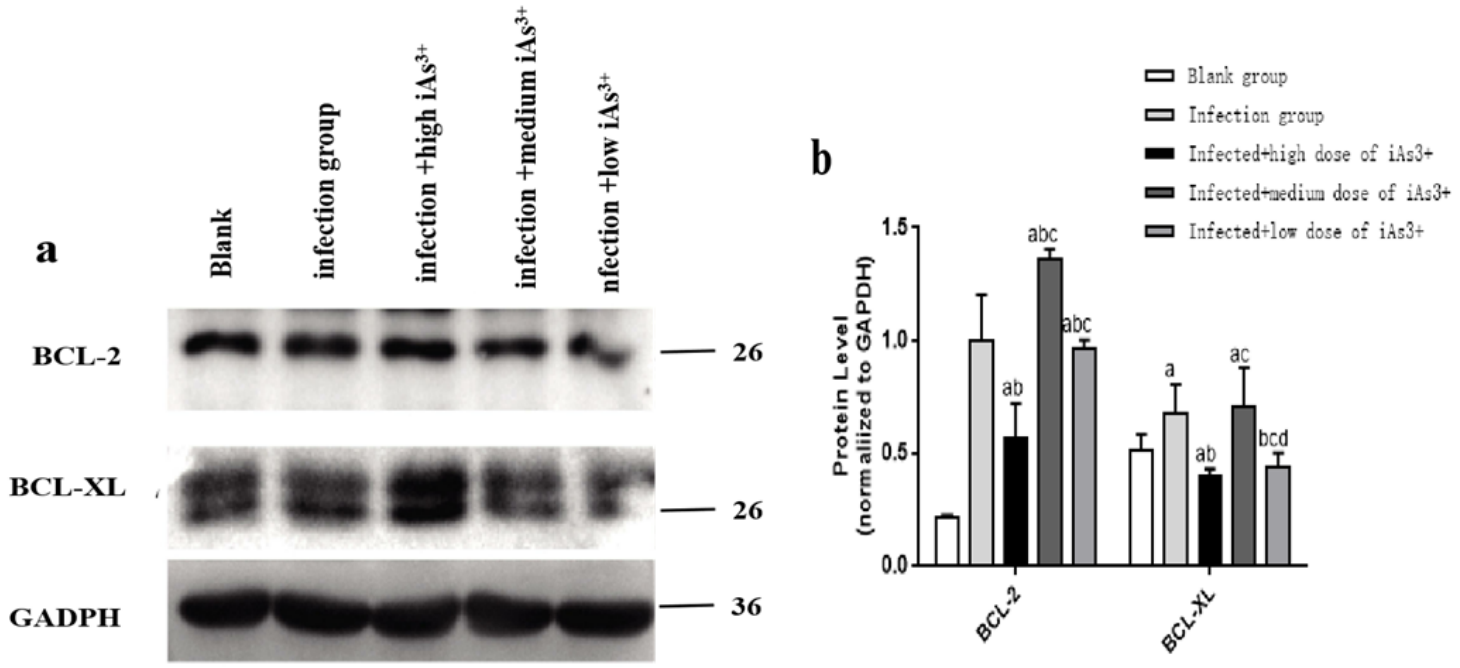

Figure 5

Western Blot data showing the sodium arsenite effects on BCL-2 and BCL-XL expression after lentivirus infection.

a) Molecular weight markers are shown on the right. b) The relative expression of BCL-2 and BCL-XL proteins (Note: different letters represent different comparisons. Compared with the blank group, $^{a}P < 0.05$; compared with the infected group, $^{b}P < 0.05$; compared with the infection + high iAs^{3+} group comparison, $^{c}P < 0.05$; and compared with the infection + medium iAs^{3+} group, $^{d}P < 0.05$).

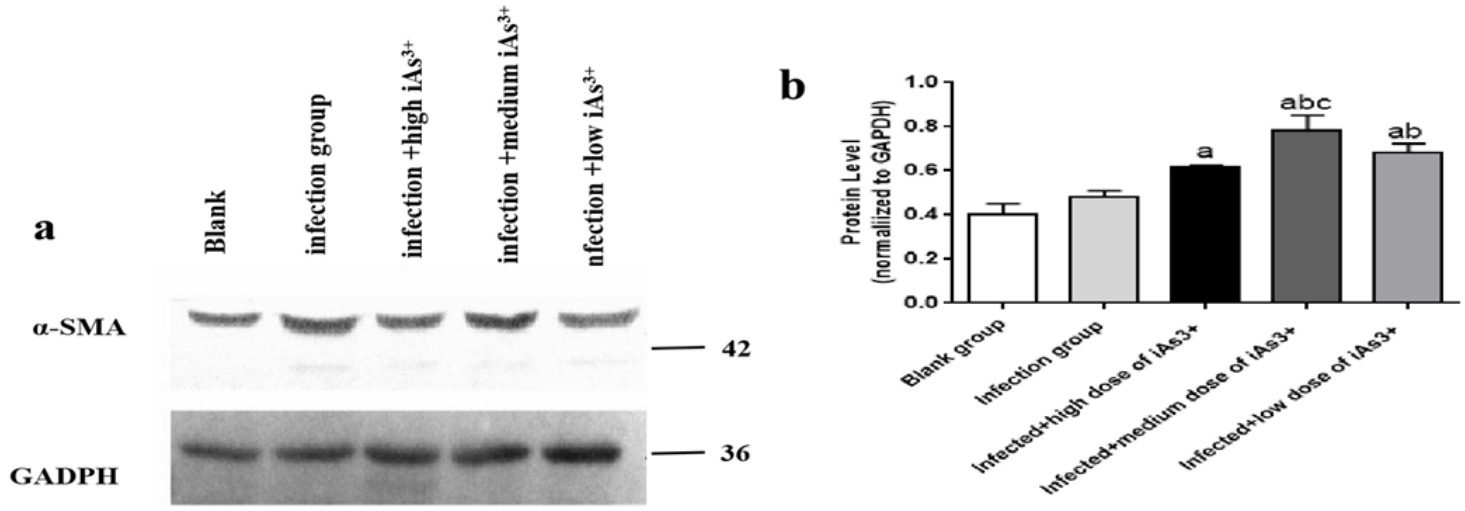

Figure 6

Western blot data showing the iAs^{3+} effects on α-SMA levels in LX-2 cells after lentivirus infection.

a) Molecular weight markers are shown on the right. b) The relative expression of α-SMA (Note: different letters represent different comparisons. Compared with the blank group, $^{a}P < 0.05$; compared with the infection group, $^{b}P < 0.05$; compared with the infection + high iAs^{3+}dose group, $^{c}P < 0.05$; and compared with the infection + medium iAs^{3+} group, $^{d}P < 0.05$).

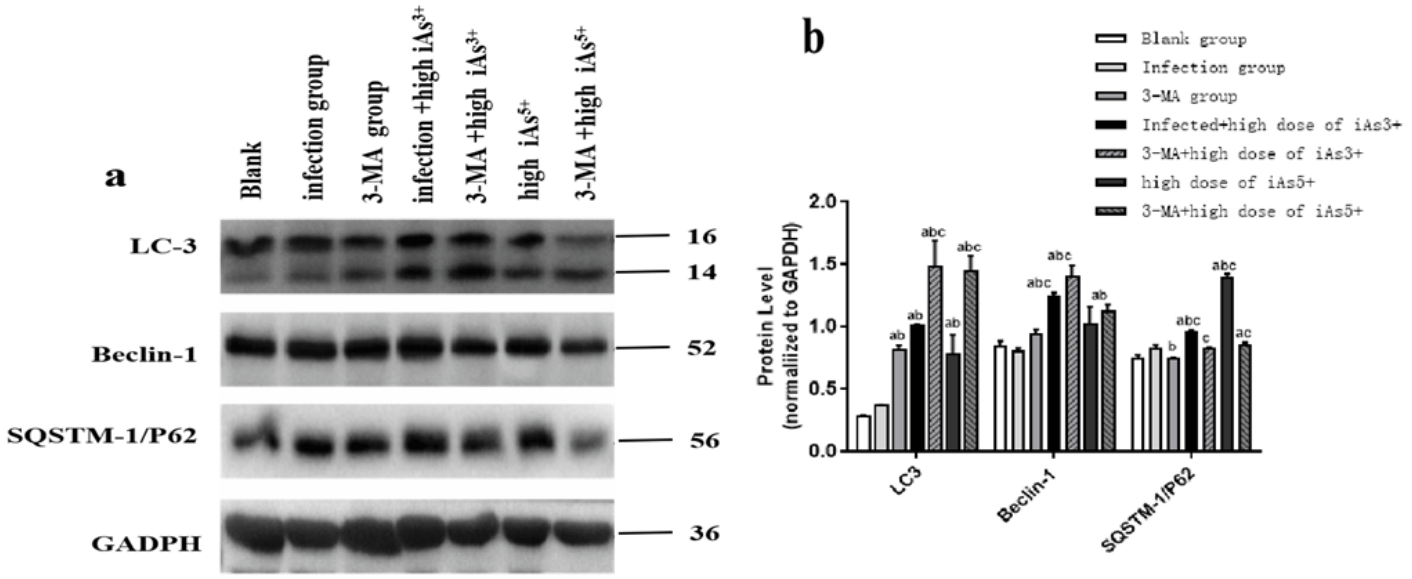

Figure 7

Western Blot data for 3-methyladenine (3-MA) combined with iAs and their effects on LC3, Beclin-1, and SQSTM-1/P62 expression in LX-2 cells after lentivirus infection.

a) Molecular weight markers are shown on the right. b) The relative expression levels of LC3, Beclin-1, and SQSTM-1/P62. (Note: different letters represent different comparisons. Compared with the blank group, $^{a}P < 0.05$; compared with the infected group, $^{b}P < 0.05$; and compared with the 3-MA group, $^{c}P < 0.05$.